4.

DESIGN AND ANALYSIS OF HIGHLY ISOLATED MINIATURIZED TRIPLE-BAND MIMO/DIVERSITY ANTENNA FOR MOBILE HANDSETS

4.1 Introduction

The MIMO technology has ability to provide higher data rate and higher quality mobile communication services by mitigating the multipath fading [Vaughan and Anderson (1987), Foschini and Gans (1998)]. In the wireless industry, the demands of low profile, multiband with multi-elements antenna system have increased rapidly. The solution of multiband antennas with multi-elements was reported in [See *et al.* (2012), Nezhad and Hassani (2010)]. In [See *et al.* (2012)], printed diversity monopole antenna for Wi-Fi/WiMAX applications was presented. The modified ground plane and neutralization line were used for wide impedance matching and improved isolation characteristics, respectively. A tri-band E-shaped printed monopole antenna was presented in [Nezhad and Hassani (2010)] for MIMO applications. The antenna operated at 2.4 GHz, 5.4 GHz, and 5.8 GHz but could not provide WiMAX frequency band. Mallahzadeh *et al.* proposed tri-band printed monopole antenna that resonates at 2.4 GHz, 3.5 GHz, and 5.2 GHz but not operating over 5.8 GHz [Mallahzadeh *et al.* (2011)]. The above reported monopoles are unable to cover all the three frequency bands i.e. WLAN, WiMAX, and HiperLAN simultaneously and also limit the applications of monopoles for mobile phone due to inherent limitation of ground plane sensitivity and back lobe radiations.

The bottleneck problem of ground plane sensitivity and back lobe radiations of the monopole antenna can be reduced by using PIFA that provides low SAR due to low back lobe radiation. Some of the PIFAs for handset application with MIMO elements were reported in [Manteghi and Rahmat-Sammi (2007), Singh *et al.* (2013a), Singh *et al.* (2013b)]. The above reported PIFAs having the multi resonant nature and operated over WLAN and HiperLAN frequency bands only,

but not cover the WiMAX frequency band and size of antennas are also large compared to the modern handsets antenna so authors' have failed to meet the demand of compactness.

However, when multiple antenna elements are closely fitted into a confined space, mutual coupling/isolation between these antennas becomes another crucial parameter that has to be taken into consideration. This kind of situation can occur in mobile communications, especially in mobile phones, where space limitations become an important variable. So it gives a real challenge to antenna designers to produce an efficient MIMO antenna system with low mutual coupling. To improve the decoupling between the antenna elements of the MIMO array various decoupling techniques were reported in [Sonkki and Salonen (2010), Meshram *et al.* (2012), Makinen *et al.* (2007), Park *et al.* (2009), Diallo *et al.* (2006), Diallo *et al.* (2007)]. In [Sonkki and Salonen (2010), Meshram *et al.* (2012)], the mutual coupling was effectively reduced by using DGS. In [Makinen *et al.* (2007)], Electromagnetic Band Gap (EBG) structure was used to reduce the mutual coupling by suppressing the surface waves. However, EBG structures require an intricate fabrication process and also a large area. In [Park *et al.* (2009)], meandered suspended line, and in [Diallo *et al.* (2006), Diallo *et al.* (2007)] neutralization line were used for isolation improvement between MIMO antennas. In above reported literatures, larger area is occupied by the MIMO antenna and suspended/neutralization line therefore, it is difficult to accommodate the camera and acoustic system of the mobile phones. In [Nakajima *et al.* (2011)], a 3-dB hybrid coupler is used for isolation improvement. This technique resulted in a bulky and complex system that limits the application in mobile phones due to limited space availability.

This chapter demonstrates a low profile tri-band PIFA for MIMO applications for mobile handsets and operating over IEEE 802.11b/g (2.42−2.48 GHz), WiMAX (3.25−3.5 GHz), and IEEE 802.11a (5.15−5.83 GHz) bands. The MIMO antenna system consists of two PIFAs. Each PIFA is constructed by a meandered line and a folded patch with two vertical parasitic strips so that it makes compact

($9\times8.8\times5.4$ mm^3) to fit into the mobile phones. This MIMO antenna system provides isolation (≤ -10dB) in free space over the operating frequency bands by properly placing the antennas on the top two corners of the PCB and selecting the positions of the feed points and shorting plate. However, when we consider the MIMO antenna in the vicinity of the mobile environment like battery, LCD, housing, camera, sensors, acoustics, and other RF circuit elements, the isolation characteristics may deteriorate. Therefore, in this chapter a MIMO antenna system with two folded shorting strips of length 0.21λ at 2.45 GHz is proposed to achieve low mutual coupling to compensate the effect of mobile environment. The folded shorting strip is connected between each antenna element (feed strip facing) and PCB ground plane at the end of antenna that makes more suitable space for placing of the mobile phone accessories like camera and speaker. The idea is to create an additional coupling path such that the ground plane current from port 1 is not entering into port 2 so that a current loop is formed between shorting pin to feed point via folded shorting strip. Thus, the amount of current flowing from port 1 to port 2 is insignificant and it leads to low mutual coupling between two antenna elements.

4.2 Antenna Configuration and Design

The antenna configuration along with fabricated prototype of the proposed MIMO antenna is shown in Fig. 4.1(a). It is composed of two symmetrical back-to-back PIFA elements, which are located on top two corners of the mobile circuit board of size 100×60 mm^2 (0.8mm thick FR4 substrate with $\varepsilon_r = 4.4$ and $\tan\delta = 0.018$). Several arrangements of antenna over PCB are possible considering which feeding or shorting strips are facing. In this design, both feeds in front of each other as this configuration is experimentally known to generate better isolation between the antennas [Diallo *et al.* (2006), Diallo *et al.* (2007)]. The antenna element is made up of copper sheet with thickness of 0.2 mm. Fig. 4.1(b)-(c) show the details of single antenna element and its optimized shape parameters. To achieve compact structure, the Main arm of antenna is folded at the edge of upper plate from bending line as shown in Fig. 4.1(b). Each element is comprised of one

main radiating arm and two side arms which resonate at 2.45 GHz, 3.4 GHz, and 5.5 GHz, respectively. The antennas are fed with Sub Miniaturization Version A (SMA) connector and feed position of Ant. 1 is (x, y =1.7mm, 8.1mm).

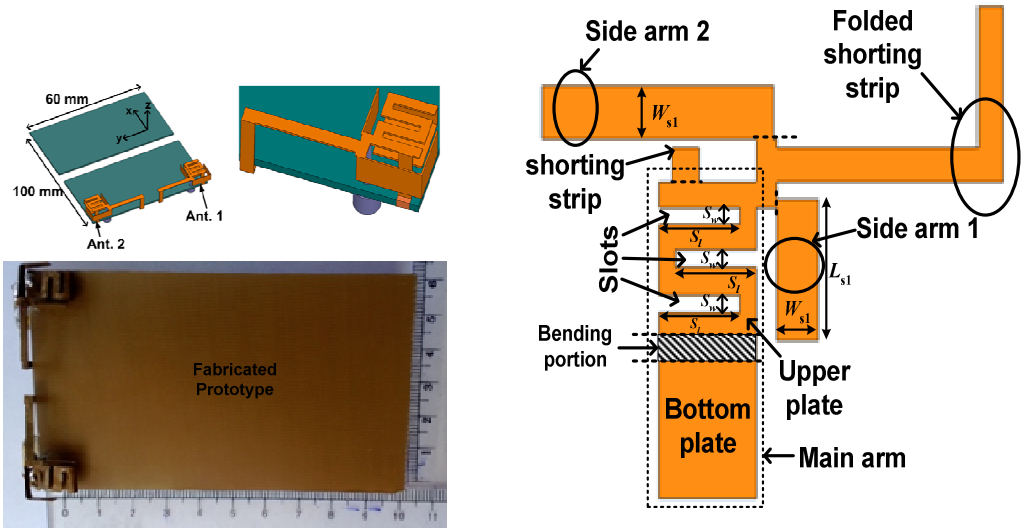

(a) (b)

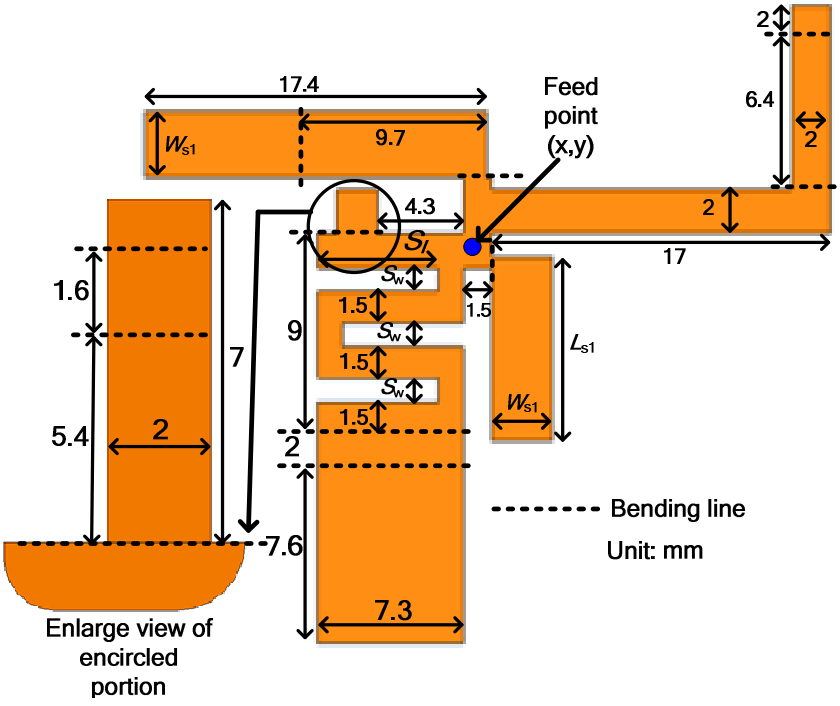

(c)

Figure 4.1: (a) Antenna configuration with zoomed structure of single antenna element and fabricated antenna, (b) Unfolded planar structure of single antenna element, and (c) Optimized dimensions of (b) (unit in mm).

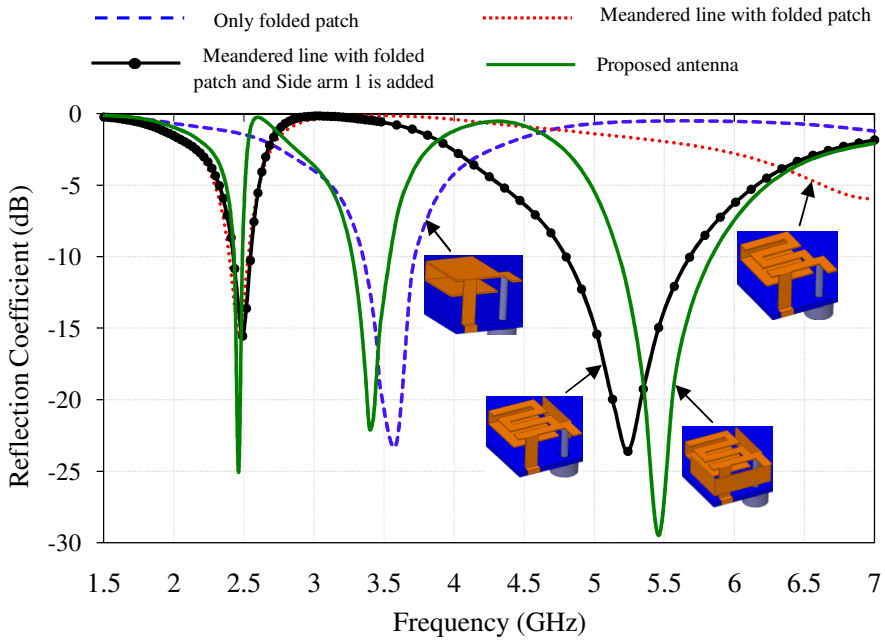

Figure 4.2: Effect of different configurations on reflection coefficient.

The design of proposed PIFA is started with equation of PIFA which is given as [Ogawa and Uwano (1994)]:

$$f_0 = \frac{c}{4\sqrt{\epsilon_r}\times(L+W+\pi d)} \tag{4.1}$$

where, c is the speed of light, ε_r is the permittivity of material (air is present between ground plane and antenna elements), L is the length of Main arm (16.6 mm), W is width of Main arm (7.3 mm), d is the diameter of probe, which is taken as 1 mm in simulation, and f_0 is the resonance frequency.

The calculated value of resonance frequency from Eq. (4.1) is 3.6 GHz which is validated through simulation by considering folded patch only i.e., there are no slots and no side arms present in the structure (Fig. 4.2). The meander line structure is introduced on the upper plate of the Main arm to increase the electrical length that decreases the resonant frequency from 3.6 GHz to 2.5 GHz as shown in Fig. 4.2. In order to achieve multiband operation by this antenna, two vertical side arms are added as shown in Fig. 4.1(b). The length and width of side arms are taken according to Eq. (4.1). With Side arm 1, the antenna resonates at 2.45 GHz (WLAN band) as well as 5.2 GHz (HiperLAN band). To additionally achieve WiMAX frequency band, vertical Side arm 2 (corresponding to λ/4 at 3.4 GHz) is

added and hence the proposed antenna resonates at 2.45 GHz, 3.4 GHz, and 5.4 GHz corresponding to the WLAN, WiMAX, and HiperLAN bands, respectively, as shown in Fig. 4.2.

4.3 Results and Discussion

The optimization of the proposed antenna is carried out on Ansoft's High Frequency Structure Simulator (HFSS) software. The details of which are discussed in the following section.

4.3.1 *S*-parameters Analysis

4.3.1.1 Parametric Analysis

Initially, some critical shape parameters of the proposed MIMO antenna are optimized for better impedance matching to get desired operating frequency bands. In order to this, length of the slot (S_l) is optimized to get the resonance at 2.45 GHz. The lower operating frequency is due to the main arm. With the increase of the S_l, the electrical length associated to the top of main arm increases, resulting in lower resonance frequency decreases as shown in Fig. 4.3. The optimized value of the S_l is 6 mm. Similarly, slot width (S_w) is optimized. The effect of S_w is shown in Fig. 4.4. When S_w increases lower operating frequency decreases because electrical length on top of the main arm increases. The optimized value of S_w is 1 mm because at this particular value the lower resonance occurred at 2.4 GHz and covers the desired operating band of WLAN. Next, the length of side arm 1 (L_{s1}) is tuned and effect is observed in Fig. 4.5. It is observed that, the side arm 1 is responsible for higher frequency band as L_{s1} increases higher frequency band decreases rapidly. The optimized value of the L_{s1} is 8.2mm for this particular value antenna resonates at 5.5 GHz of higher frequency band. Again, width of side arms (W_{s1}) is tuned and shown in Fig. 4.6. The width of both side arms are same due to which width of arms mainly affect the WiMAX and HiperLAN bands. The side arm 1 is responsible for HiperLAN band while side arm 2 is responsible for WiMAX band. As the width of the slot increases resonant frequency of both bands increase. The tuned value of W_{s1} is 3mm.

4.3.1.2 Simulated and Measured *S*-parameters

After successful optimization of shape parameters using HFSS, the optimized results are validated with other simulation software i.e., CST MWS and the MIMO antenna is fabricated. The fabricated prototype is tested on Agilent Technology (E8364B, 10 MHz – 50 GHz) Network Analyzer. The simulated and measured results are shown in Fig. 4.7, which are in good agreement. Some discrepancies between simulated and measured results are

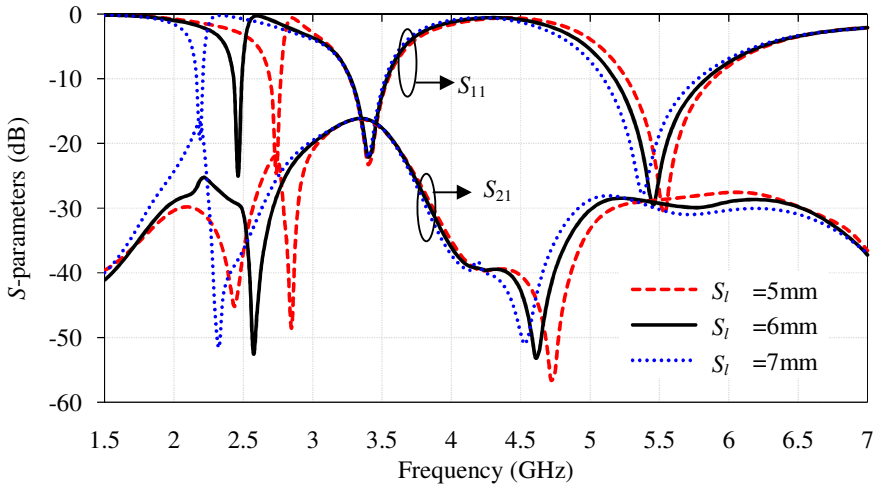

Figure 4.3: Effect of slot length (S_l) on *S*-parameters.

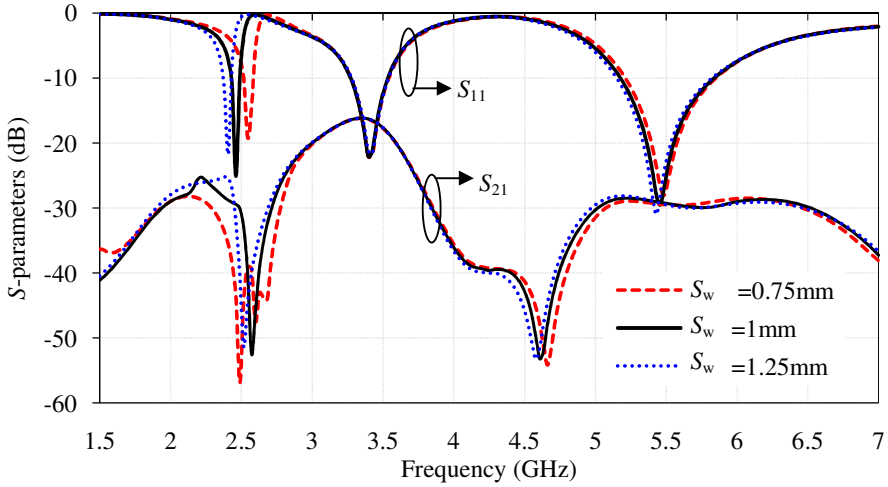

Figure 4.4: Effect of slot width (S_w) on *S*-parameters.

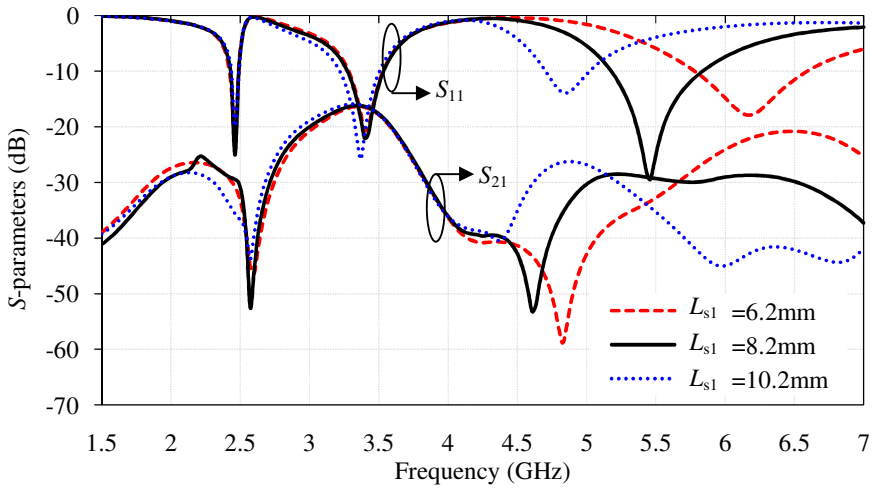

Figure 4.5: Effect of length of the side arm 1 (L_{s1}) on *S*-parameters.

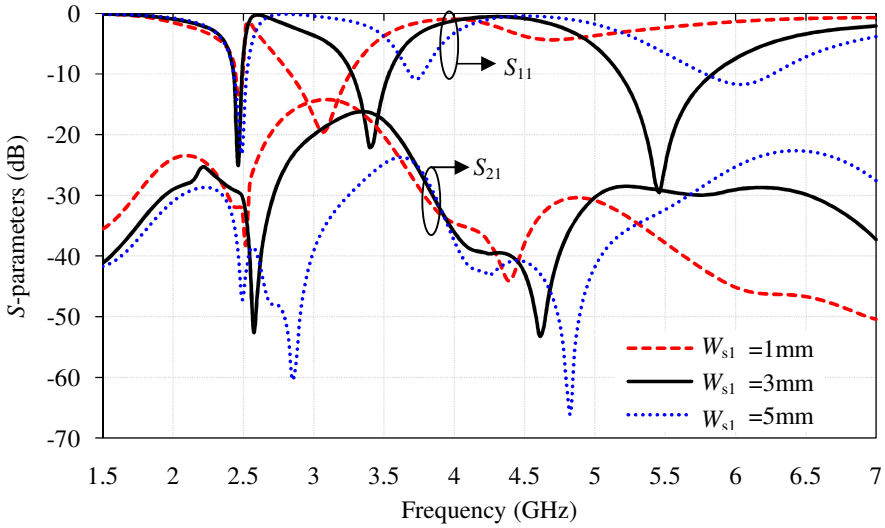

Figure 4.6: Effect of width of the side arms (W_{s1}) on *S*-parameters.

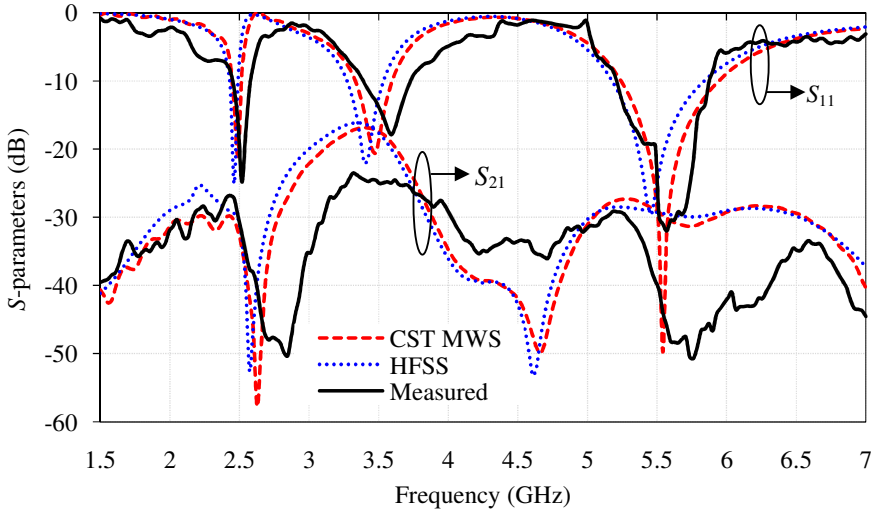

Figure 4.7: Simulated and measured results of *S*-parameters in free space.

observed. This is due to manual fabrication and improper adjustment of the air gap. Further, CST MWS simulation software is used to obtain surface current distributions, far-field radiation patterns along with the diversity parameters of the proposed antenna and also used to analyse the antenna performances in the user proximity.

4.3.1.3 Effect of Mobile Environment and User Proximity on *S*-parameters

After the study of *S*-parameters in free space, the effect of mobile environment and user proximity (SAM head + PDA hand "Talk mode") on reflection and coupling *S*-parameters of the MIMO antenna are studied. Fig. 4.8 shows the typical environment of multimedia mobile phone. The mobile environment comprises the large size touch screen LCD, battery, camera of diameter 8.5 mm and thickness is 6 mm, and speaker. The position of speaker is opposite side to the camera with dimension of 8.5 mm width and 18 mm length, respectively. A large size LCD of volume $73 \times 47 \times 2$ mm^3 and a battery of volume $65 \times 47 \times 3$ mm^3 are settled parallel with a spacing of 1 mm and are connected with the main PCB via connectors. All these components are assumed as Prefect Electric Conductor (PEC) during the simulation. The small metallic components like three buttons and one microphone are also considered PEC which are far from antenna elements. All these components and antenna elements are covered with a 1 mm thick plastic box of dielectric constant 3 and conductivity 0.02 S/m which form housing of the mobile phone. The simulation setup of mobile environment and user proximity are modelled in CST MWS.

The variation of *S*-parameters are plotted by considering the antenna without folded shorting strip in free space as well as in presence of mobile components and user proximity as shown in Fig. 4.9. It is observed that both reflection and coupling *S*-parameters are less affected by the user proximity and mobile environment at lower frequency band whereas the resonance frequencies of the WiMAX and HiperLAN bands are shifted but still cover the entire operating bands with reference to -6 dB reflection coefficient. The occupied bandwidth of the proposed antenna based on -6dB reflection coefficient is (2.39-2.5 GHz) of

WLAN, (3.16-3.63 GHz) of WiMAX, and (5.03-6.13 GHz) of HiperLAN bands. Also the coupling *S*-parameter is much deteriorated in the user proximity (Talk mode).

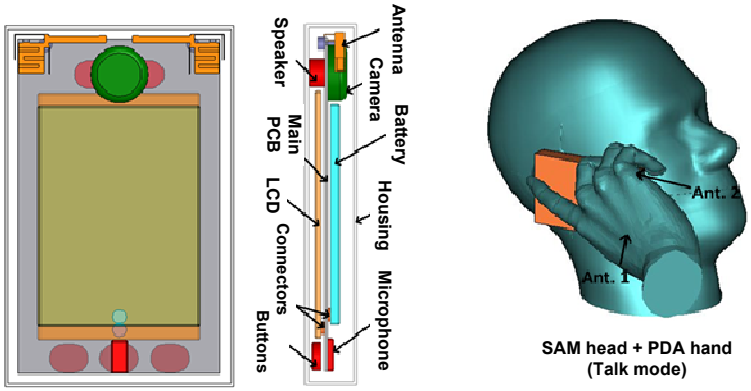

Figure 4.8: Configuration of the mobile phone with user proximity.

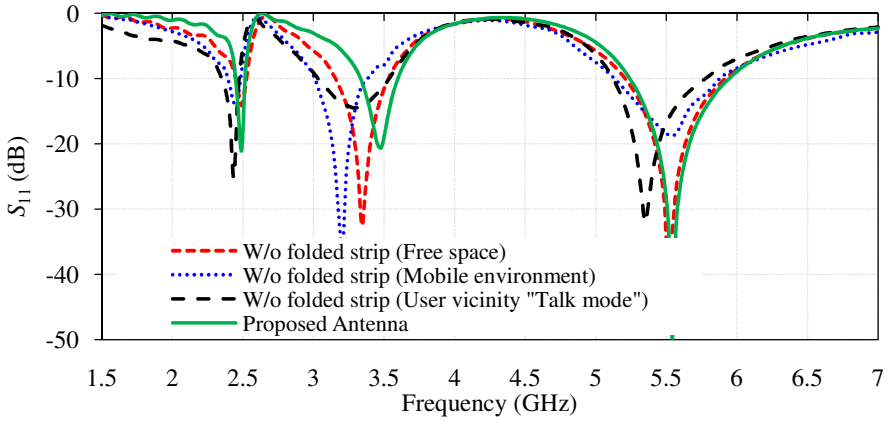

(a)

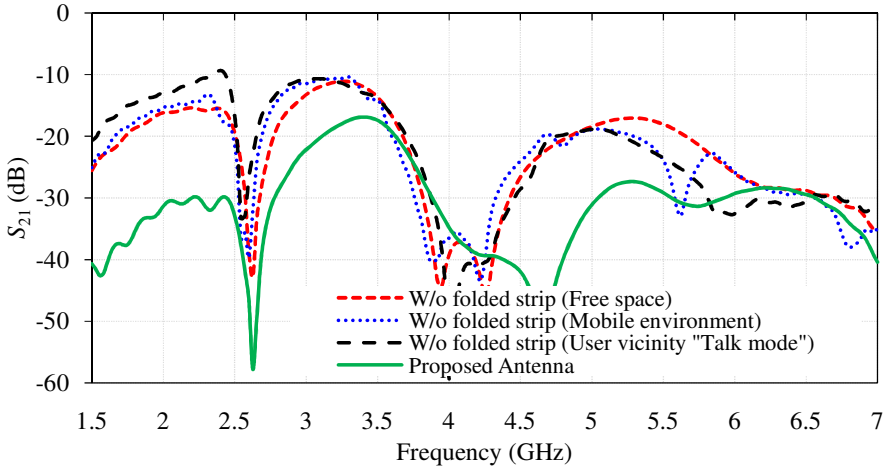

(b)

Figure 4.9: Variation of *S*-parameters without folded shorting strip in different environment, (a) S_{11} and (b) S_{21}.

In view of the above, it is necessary to enhance the isolation between MIMO antenna when antenna is placed in the mobile environment, a subsequent structure shown in Fig. 4.1 is proposed, which employs a folded shorting strip to reduce the surface current flow between two antenna elements on the ground plane. The main role of folded shorting strip is to make a current loop to avoid the current flow from port 1 to port 2 so that low mutual coupling is achieved. The optimized length of the folded shorting strip is obtained 25.4 mm i.e. 0.21λ at 2.45 GHz. Fig. 4.10 shows the simulated reflection and coupling *S*-parameters of the proposed antenna in free space as well as in the presence of mobile components and user proximity (Talk mode). The achieved isolation values with the proposed structure are below -13 dB over all the operating frequency bands when it placed in the user proximity with mobile environment. Enhancement in the isolation as compared to the MIMO antenna without folded shorting strip (refer Fig. 4.9) is 11 dB at WLAN band, 4 dB at WiMAX band, 14 dB at HiperLAN band is observed in the case of free space and mobile environment whereas significant improvement is also observed for user proximity (Talk mode) case.

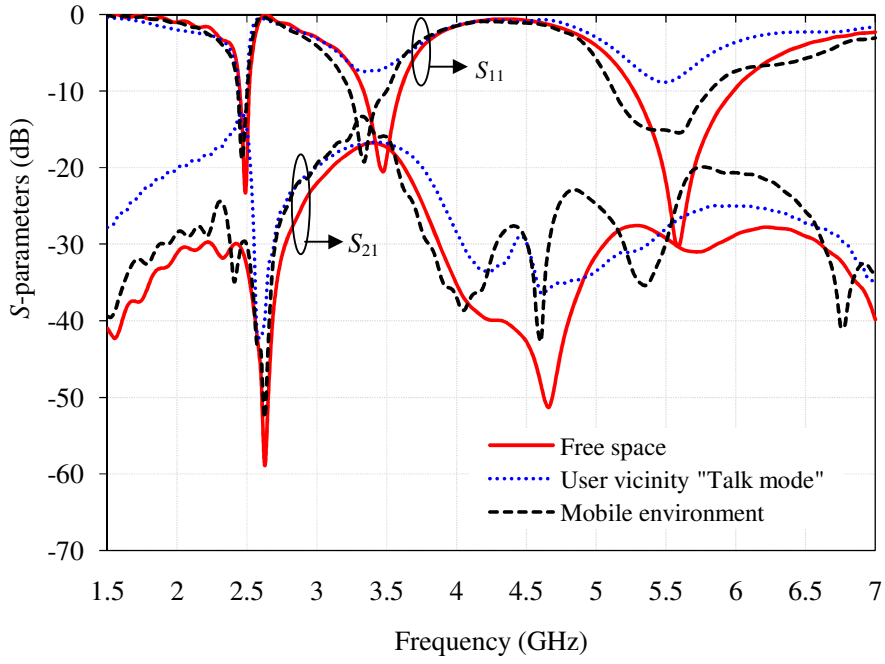

Figure 4.10: Variation of *S*-parameters of the proposed antenna in different environment.

4.3.2 Surface Current Distribution

To investigate the mechanism of the folded shorting strip, surface current distributions on the proposed antenna at different resonance frequencies are plotted when one antenna is excited (Ant. 1) while the other (Ant. 2) is terminated with 50 Ω matched load. Fig. 4.11 illustrates that without folded shorting strip structure, a small amount of surface current is coupled from Ant. 1 to Ant. 2 through common ground plane. This surface current flow between two ports is reduced to a great extent by the folded shorting strip at all the above mentioned frequencies and also the effect is same when Ant. 2 is excited and Ant. 1 is matched terminated. From Fig. 4.11, it is clearly shown that very less amount of current is flowing towards port2 and maximum amount of ground current is flowing into folded shorting strip and towards feed point. So that the folded shorting strip can significantly increase the isolation of MIMO antenna system.

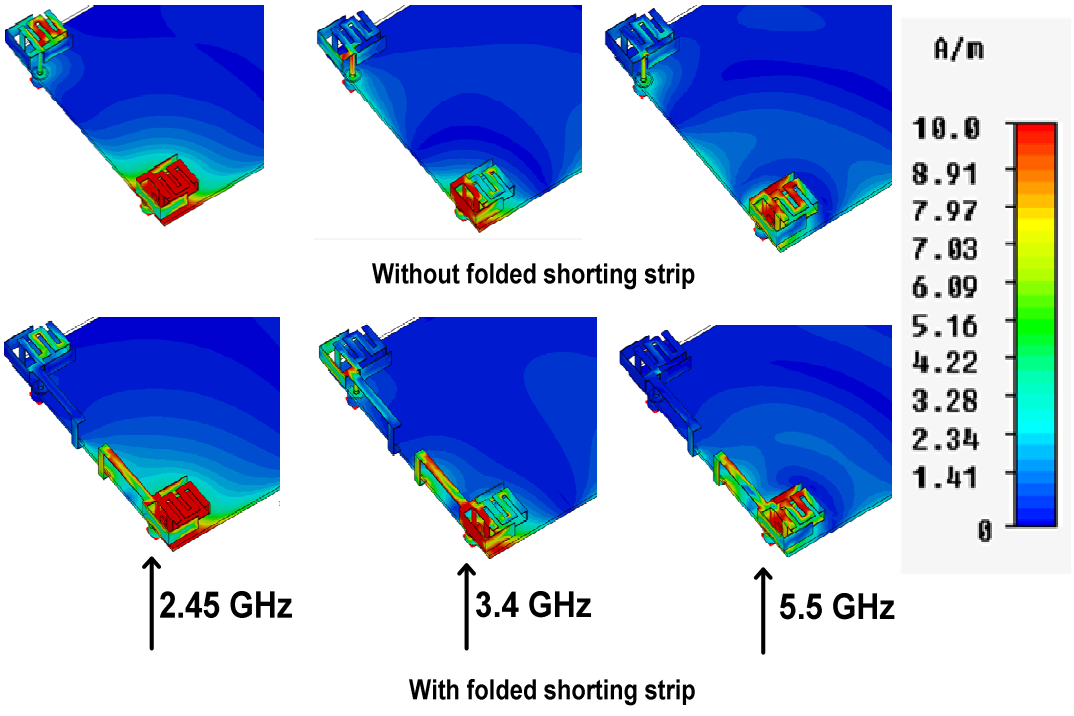

Figure 4.11: Surface current distribution (with and without folded shorting strip) when Ant. 1 is excited while Ant. 2 is matched terminated with 50 Ω load.

4.3.3 Radiation Performances

The simulated 3D far-field radiation patterns are obtained using CST MWS and the results are shown in Fig. 4.12(a). In the case of MIMO antenna system only one port is excited while keeping other port matched terminated with 50 Ω load. The radiation patterns of Ant. 1 and Ant. 2 are almost mirror images of each other over all the operating frequency bands. That means they are covering the complementary space regions and indicating that the proposed MIMO antenna has good pattern diversity characteristics.

To verify the pattern diversity of simulated 3D far-field radiation patterns, 2D far-field radiation patterns are measured at different resonating frequencies (2.45 GHz, 3.4 GHz, and 5.5 GHz). The measured radiation patterns (Horizontal and Vertical components) are complementary in space that verifies the pattern diversity phenomenon of the proposed antenna. During the course of measurement, only one antenna is excited while other antenna is matched terminated with 50 Ω load. The measured total field patterns of the proposed triple band MIMO antenna are shown in Fig. 4.12(b).

The symmetrically placed MIMO antenna elements having equal peak realized gain and total antenna efficiency. The peak realized gain of the proposed antenna is measured over the entire band of operations. It is observed that the measured peak realized gain lies between 2 dBi to 4.3 dBi in WLAN band, 4.25 dBi to 6 dBi in WiMAX band, and 5 dBi to 7.6 dBi in HiperLAN band as shown in Fig. 4.13(a). The variation of calculated total antenna efficiency is shown in Fig. 4.13(b). It is found that the total efficiency lies between 40% to 90% in WLAN band (2.39-2.5 GHz), 76% to 95% in WiMAX band (3.16-3.63 GHz), and 70% to 96% in HiperLAN band (3.03-6.13 GHz).

4.3.4 Diversity Parameters Analysis

All the diversity parameters (ECC, MEG, and EDG) for the proposed triple-band highly isolated MIMO/Diversity antenna are calculated using CST MWS. The details of which are given in the following sections.

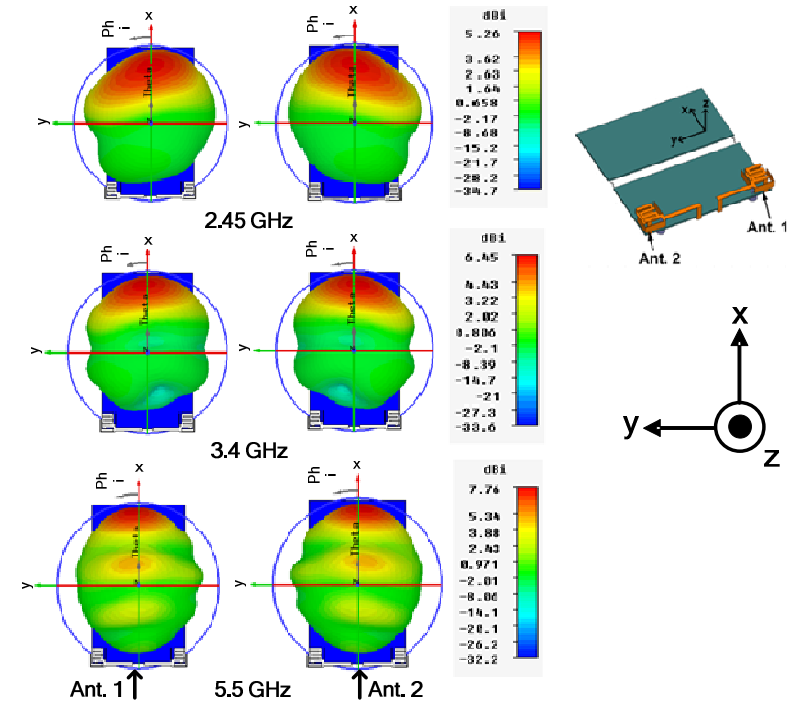

(a)

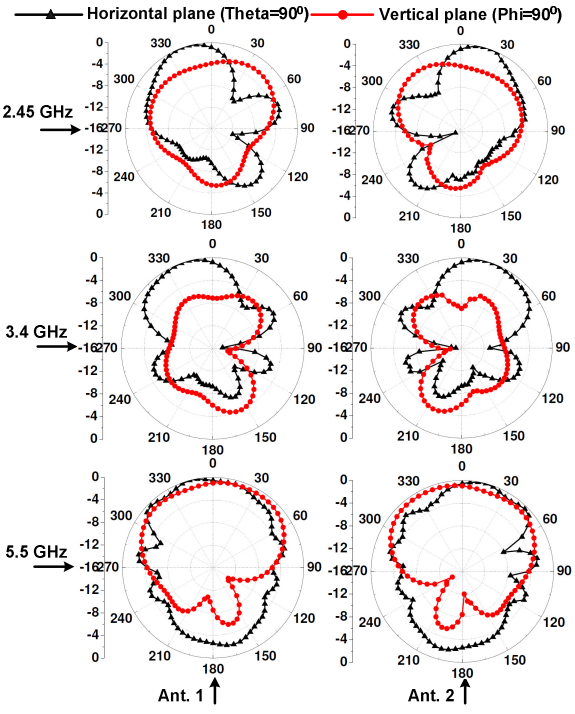

(b)

Figure 4.12: (a) Simulated 3D far field radiation patterns at different resonance frequencies and (b) Measured 2D far field radiation patterns at different resonance frequencies.

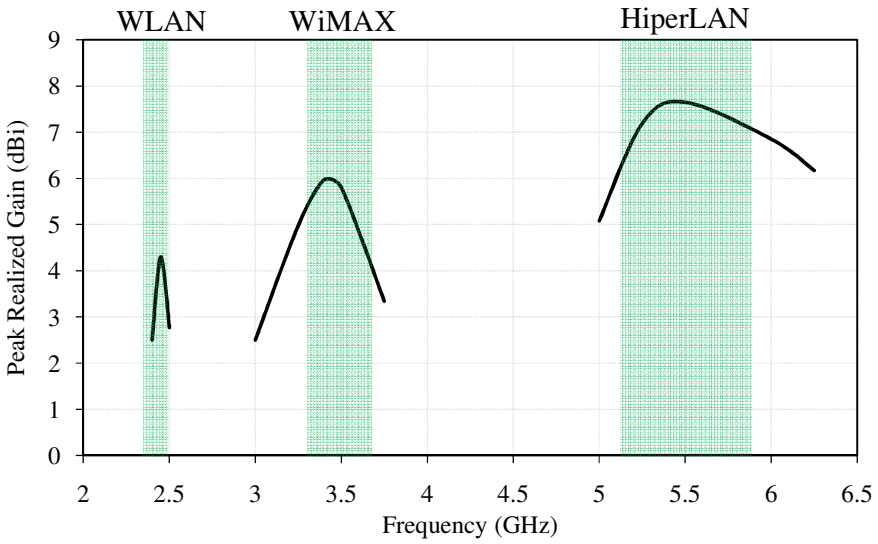

(a)

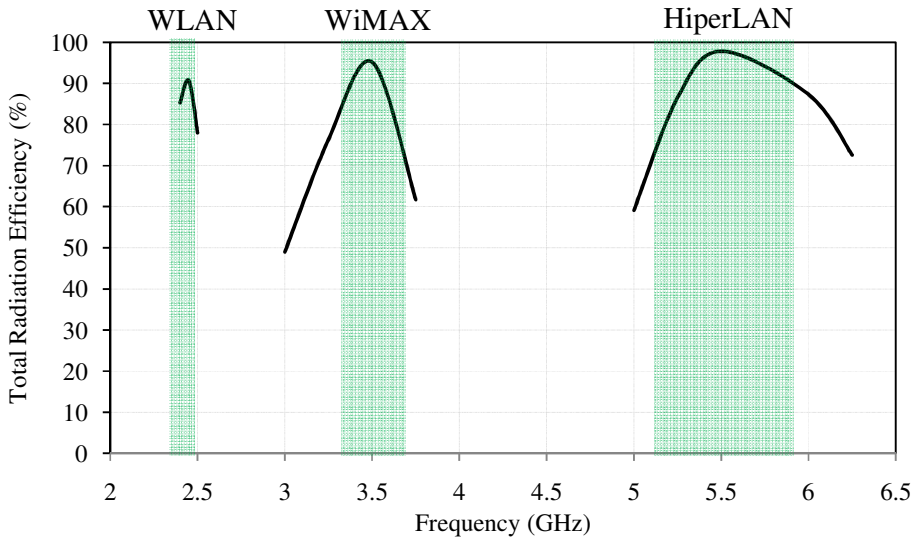

(b)

Figure 4.13: (a) Variation of measured peak realized gain and (b) Total antenna efficiency with frequency.

4.3.4.1 Envelope Correlation Coefficient (ECC)

To calculate ECC, can approach either *S*-parameters method or far field pattern data methods. In this thesis, far field pattern data approach is followed. Fig. 4.14 shows the variations of calculated ECC with frequency. It can be observed that the ECC values are less than 0.1 for the operating frequency bands, which is well within the maximum allowed limit (0.5).

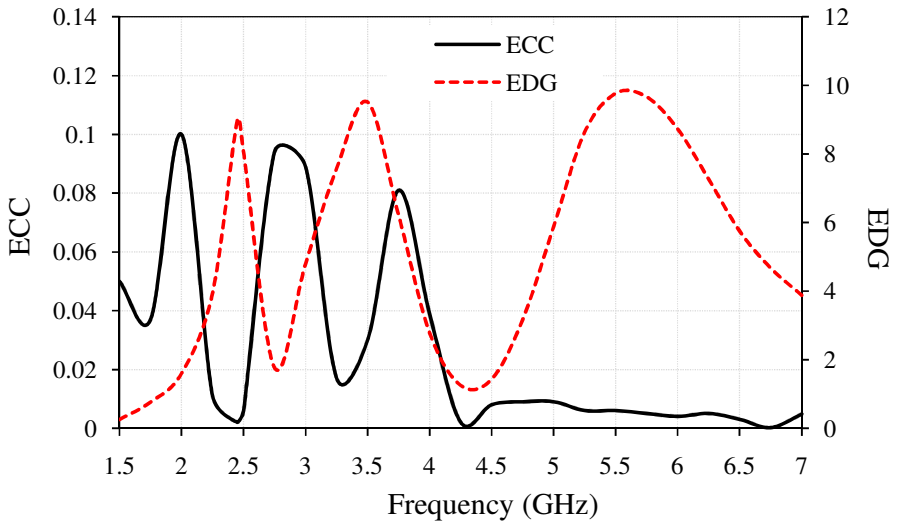

Figure 4.14: Variation of ECC and EDG with frequency.

4.3.4.2 Mean Effective Gain (MEG)

The MEG of the proposed antenna is calculated by using Eq. (2.4) which is given as [Taga (1990)]:

$$MEG = \int_0^{2\pi}\int_0^{\pi}\left[\frac{XPR}{1+XPR}G_\theta(\theta,\phi)P_\theta(\theta,\phi) + \frac{1}{1+XPR}G_\phi(\theta,\phi)P_\phi(\theta,\phi)\right]sin\theta d\theta d\phi$$

Table 4.1 shows the computed MEG in free space for different *XPR* at different frequency bands by setting the, m_v=10^0, m_H=10^0, σ_v=15^0, and σ_H=15^0. By observing the table, it is clearly seen that ratio of the MEG1/MEG2 is nearly equal to unity which satisfy the equality criterion of the two antennas. The slight difference between MEG1 and MEG2, considering the fact that the two antennas are identical, is due to the difference in the gain patterns at the assumed angle for the incident power.

4.3.4.3 Effective Diversity Gain (EDG)

The effectiveness of diversity is given in terms of diversity gain. Diversity gain is calculated using Eq. (2.19) [Schwartz (1965)].

$$DG = 10\sqrt{1-|ECC|^2}$$

Table 4.1: Calculated values of MEG at different frequencies.

Freq. (GHz)	Indoor (XPR=5 dB)		Outdoor (XPR=1 dB)		Isotropic (XPR=0 dB)	
	MEG1	MEG2	MEG1	MEG2	MEG1	MEG2
2.45	-5.31	-5.24	-4.64	-4.55	-4.46	-4.38
	MEG1/MEG2=1.01		MEG1/MEG2=1.02		MEG1/MEG2=1.02	
3.5	-5.30	-5.29	-4.76	-4.77	-4.6	-4.59
	MEG1/MEG2≈1		MEG1/MEG2=0.99		MEG1/MEG2≈1	
5.25	-3.24	-3.25	-3.82	-3.82	-3.99	-3.99
	MEG1/MEG2=0.99		MEG1/MEG2=1		MEG1/MEG2=1	

The apparent diversity gain which is based on selection combining with respect to 1% distribution level does not include the antenna radiation efficiency. So we failed to achieve effectiveness of diversity capability without considering antenna efficiency into account. In view of this, the *EDG* is calculated by multiplying the total efficiency by *DG* and formula given in Chapter 2 (Eq. 2.21). The EDG is plotted with frequency in Fig. 4.14.

4.3.5 Analysis of SAR and TRP in User Proximity

The human head phantom near to the mobile phone are placed according to the CTIA standard [CTIA Report (2011)] and shown in Fig 4.15. The dielectric properties of the human tissues are given in Table 4.2.

As our previous discussion, the MIMO antenna has more operation mode, which also bring new problem for evaluating the antenna's SAR. The mutual coupling between the multi elements will change the distribution of current density, and influence the SAR value. When the dual antennas operate simultaneously, FCC standard, the value of SAR to PEAK Location Spacing Ratio (SPLSR) is utilized to evaluate the SAR performance [FCC Report (2008)]. In the calculation of SPLSR, the SAR1 and SAR2 are related to Antenna 1 and Antenna 2, respectively. The separation distance of the two SAR peaks and values of SAR are calculated using CST MWS simulation software. The calculation of SAR is

done over 1g and 10g average human tissue. The SPLSR is calculated at three different resonating frequencies i.e. 2.45 GHz, 3.5 GHz, and 5.25 GHz. The incident power for SAR calculation is 21dBm for 2.45GHz and 3.5GHz and 17dBm for 5.8GHz chosen [CTIA Report (2005)]. The distribution of electromagnetic energy inside the human tissue is shown in Fig. 4.16. The calculated values of SPLSR are given Table 4.3. It is observed that the calculated values of SPLSR are well below the defined limit by FCC i.e. 0.3.

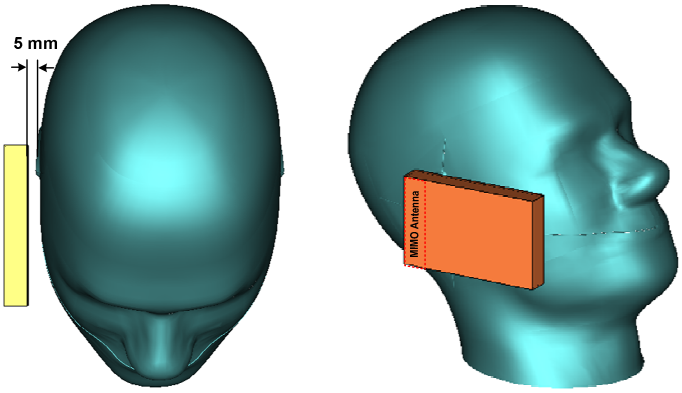

Figure 4.15: SAR simulation setup according to CTIA.

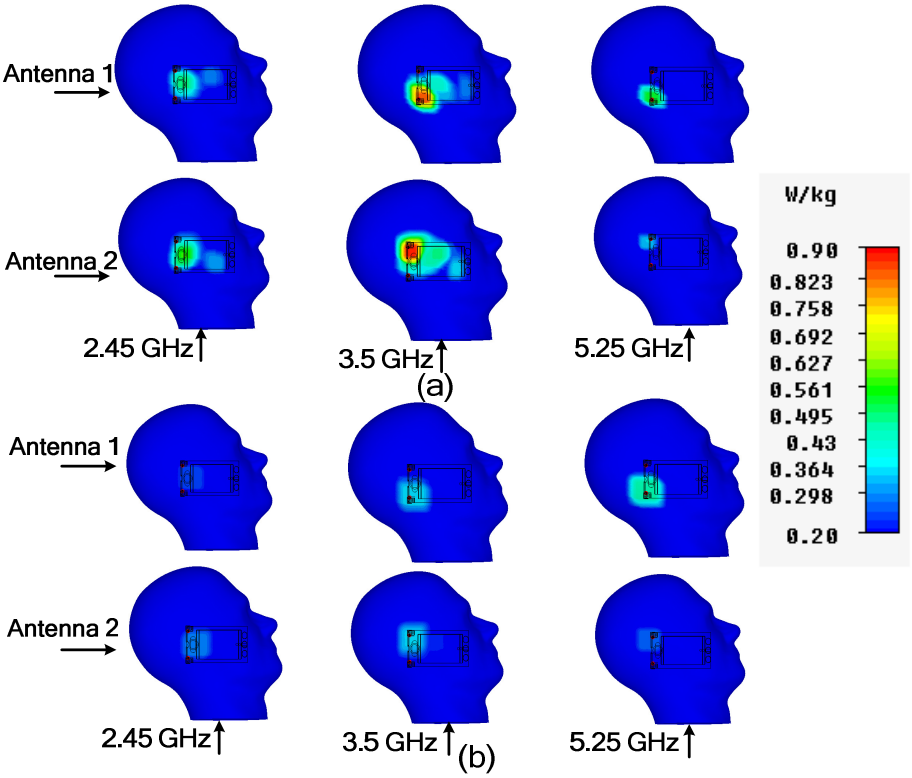

Figure 4.16: Distribution of energy over human tissue, (a) Average SAR over 1g and (b) Average SAR over 10g.

In the case of multi element MIMO system, the TRP is calculated of each element of MIMO antenna system and defined as TRP1 and TRP2 of Antenna 1 and Antenna 2, respectively. The TRPs are calculated in free space as well as in user proximity and given in Table 4.4. It is ascertained that in the case of free space, TRP of Antenna 1 and Antenna 2 are same due to the uniform environment around the MIMO antenna elements. Due to the low reflection loss and high total efficiency the TRPs in free space is high i.e. more than 26 dBm. When we implement proposed antenna in real scenario the TRP decreases due to the large human body coverage around antenna elements but still better than 24 dBm. The higher TRP can significantly improve the call performance of the handset in a weak signal area.

Table 4.2: Dielectric properties of the human head tissues.

Frequency (GHz)	Human Head Tissue	
	ε	σ (S/m)
2.45	39.2	1.8
3.5	38	2.9
5.2	36	4.65
5.8	35.4	5.06

Table 4.3: SAR performances of MIMO antenna.

Distribution of SAR over 1-g tissue					Distribution of SAR over 10-g tissue			
Freq. (GHz)	SAR_1 (W/kg)	SAR_2 (W/kg)	Separation distance b/w SAR peaks (D) unit in centimetre (cm)	SPLSR $=\frac{(SAR_1+SAR_2)}{D}$ (W/kg/cm)	SAR_1 (W/kg)	SAR_2 (W/kg)	Separation distance b/w SAR peaks (D) unit in centimeter (cm)	SPLSR $=\frac{(SAR_1+SAR_2)}{D}$ (W/kg/cm)
2.45	0.49	0.56	3.5	0.29	0.25	0.29	2.16	0.25
3.5	0.85	0.86	5.7	0.3	0.36	0.35	3.77	0.19
5.25	0.53	0.34	3.67	0.24	0.47	0.27	3.74	0.197

Table 4.4: Calculated values of TRP for proposed MIMO antenna in free space and user proximity.

Frequency (GHz)	Free Space		User Proximity	
	TRP1 (dBm)	TRP2 (dBm)	TRP1 (dBm)	TRP2 (dBm)
2.45	26.2	26.2	25.25	25.05
3.5	26.7	26.7	24.55	24.4
5.25	26.3	26.3	25.86	25.7

4.4 Summary

A miniaturized triple-band highly isolated MIMO antenna is designed and investigated for WLAN, WiMAX, and HiperLAN applications. The implementation of non-radiating folded shorting strips between MIMO antenna elements successfully minimizing the effect of large metallic components and user presence on the *S*-parameters. By the use of folded shorting strip, the isolation between MIMO antenna elements is still below -13 dB in the presence of mobile phone components and user. The simulated and measured *S*-parameters results are found in close agreement and cover the desired frequency bands. The radiation patterns of the proposed antenna in free space show pattern diversity which is suitable for mobile communication to mitigate the multipath fading. The diversity parameters of the proposed antenna have also been evaluated in free space and obtained good results. In the presence of user's body SPLSR and TRP are calculated and found within the standard limit.

After completion of the study of miniaturized triple-band diversity antenna, compact quad-band diversity antenna for next generation (4G) mobile handsets is investigated numerically and experimentally in the chapter five.